ELSEVIER

Chemical Engineering Journal 134 (2007) 180–189

Chemical Engineering Journal

www.elsevier.com/locate/cej

Transient behavior of the methane partial oxidation in a short contact time reactor: Modeling on the base of catalyst detailed chemistry

N.V. Vernikovskaya [a,c,*], L.N. Bobrova [a,c], L.G. Pinaeva [a], V.A. Sadykov [a,c], I.A. Zolotarskii [a], V.A. Sobyanin [c], I. Buyakou [b], V. Kalinin [b], S. Zhdanok [b]

[a] *Boreskov Institute of Catalysis, Pr. Akademika Lavrentieva, 5, Novosibirsk 630090, Russia*
[b] *Heat and Mass Transfer Institute of the National Academy of Sciences of Belarus, 15, P. Brovka, Minsk 220072, Belarus*
[c] *Novosibirsk State University, 2, Pirogova St., Novosibirsk 630090, Russia*

Abstract

The objective of the paper is a numerical study of the partial oxidation of methane to synthesis gas in a monolith reactor with Pt/Ce-Zr-La catalyst. A dynamic one-dimensional two-phase reactor model of the processes with accounting for both transport limitations in the boundary layer of a fluid near the catalyst surface and detailed molecular unsteady-state kinetic model for surface reactions have been developed and verified with the transient experiments data. The mathematical model was used to explain a transient behavior of the process in the monolith reactor during start-up (ignition). Also studied is the influence on the process dynamics such parameters as linear velocity, equivalent diameter of triangular channel and effective thermal conductivity of the monolith. It was found that higher linear velocity and equivalent channel diameter as well as the worse axial conductivity of solid phase favor decreasing a time delay in syngas production in the Pt/Ce-Zr-La/α-Al_2O_3 honeycomb monolith with a triangular shape channels.
© 2007 Elsevier B.V. All rights reserved.

Keywords: Methane; Air; Partial oxidation; Monolith reactor; Platinum; Simulation

1. Introduction

It is known that during the partial oxidation of hydrocarbons in a monolith reactor at short contact time ($\leq$0.1 s), ignition is characterized by a sharp increase in the surface temperature in the front part of the catalytic bed. Moreover, radial and axial temperature gradients may also develop in a monolithic catalyst [1–4]. The sharp temperature profile taken along the reactor axis makes the temperature in the front part of a catalytic monolith to differ markedly from the outlet temperature. Also, throughout the cross-section, even at the monolith diameter of a few centimeters, the radial gradients of 100–200° could be observed. The high temperature over the catalyst is a major threat to the stability of supported noble metal catalyst: the catalyst may sinter, lose activity and, most importantly, the exposure of noble metals to oxygen at these temperatures will form volatile oxides resulting in the metal loss. The catalyst temperature is defined by a complex interaction of reaction kinetics on the specific catalyst and transport processes. Main properties of the methane partial oxidation in a short contact time monolith reactor were formulated by Schmidt in [2]:

- all properties of gases vary by a factor of more than 10 between feed and reactor conditions;
- most reaction occurs within one cell diameter where properties are varying;
- surface reaction events may be different than those calculated or measured at lower temperatures;
- very large temperature and concentration gradients exist in these experiments;
- radial and axial concentration gradients cause quite unpredictable conditions for homogeneous reaction and flames;
- homogeneous reactions and flames are tightly coupled to the presence of surface reactions and to cold or to hot surfaces which can alter free radical concentrations;
- multiple steady states may be expected in these systems for both homogeneous and heterogeneous processes;
- transitions between different steady states may be expected in these experiments which may lead to quite different behavior for nearly the same geometries or conditions.

* Corresponding author. Tel.: +7 3833 397558; fax: +7 3833 308056.
E-mail address: vernik@catalysis.nsk.su (N.V. Vernikovskaya).

1385-8947/$ – see front matter © 2007 Elsevier B.V. All rights reserved.
doi:10.1016/j.cej.2007.03.072

Nomenclature

c_p	heat capacity, (J kg^{-1} K^{-1})
D_{im}	mixture-averaged diffusion coefficient between species i and the remaining mixture (m^2 s^{-1})
d_{eq}	equivalent channel diameter (mm)
D_i^T	thermal diffusion coefficients of ith compound (kg m^{-1} s^{-1})
E_f, E_b	activation energies of forward and back reactions (kcal/mol)
f_{Pt}	the molar site density for Pt (mol m^{-2})
ΔH_j	heat of reaction j (J mol^{-1})
J_i	mass flux of ith compound (kg m^{-2} s^{-1})
k_f	preexponential (s^{-1}) or sticking coefficient of forward reactions
k_b	preexponential (s^{-1}) of back reactions
m	exponent in diffusion coefficient temperature dependence
M_i	molecular weight of ith compound (kg mol^{-1})
Nu	Nusselt number
P	pressure (Pa)
Pr	Prandtl number, $Pr = \mu c_p / \lambda$
r_j, $\hat{r}_j$	jth reaction rate in gas and solid phase (g m^{-3} s^{-1}), (mol mol$_{pt}^{-1}$ s^{-1})
Re	Reynolds number, $Re = v d_{eq} \rho_g / \mu$
S_{sp}	specific surface area (m^{-1})
S_c	specific surface area occupied with Pt (m^{-1})
Sc	Schmidt number, $Sc = \mu / \rho_g / D_{im}$
Sh	Sherwood number
t	time (s)
T	temperature (K)
u	superficial velocity (m s^{-1})
x_i	mole fraction in gas phase
z	reactor axial coordinate (m)
z^*	dimensionless axial coordinate

Greek letters

α	heat transfer coefficient (J m^{-2} s^{-1} K^{-1})
β	mass transfer coefficient (m s^{-1})
ε, $\hat{\varepsilon}$	void fraction in monolith and in coverage pores
ε'	emission coefficient
λ_{eff}	effective heat dispersion coefficient (J m^{-1} s^{-1} K^{-1})
μ_{ij}, ν_{ij}	stoichiometric coefficients
μ	viscosity (kg m^{-1} s^{-1})
θ_j	surface coverage
ρ_g, $\hat{\rho}_g$	mass density in gas phase and in coverage pores (kg m^{-3})
σ	Stefan–Boltzmann constant (J m^{-2} s^{-1} K^{-4})
υ	interstitial velocity (m s^{-1})
ω_i, $\hat{\omega}_i$	weight fraction in gas phase and in coverage pores.

Subscripts

g	gas phase
in	inlet
mix	mixture
o	initial
out	outlet
s	solid phase
w	surrounding

Fundamental understanding of the processes occurring in the multiscale levels, their interrelation and interaction is essential to control such intensive, fast reaction in a specific reactor. Information about dynamics of the local temperature and concentrations may have a considerable influence on rational design of both reactor and catalyst as well as the choice of design materials. By the mathematical simulation studies the process in the monolith reactor may be examined in details. For correct mathematical modeling it is necessary to create a reliable, valid mathematical model providing for a good agreement between numerical and experimental data and accounting for all particularities of the complicated reaction kinetics. These models should be able not only to explain physicochemical processes in the reactor, but predict the behavior of reacting system. The multidimensional models, in which energy and mass balances are coupled to the Navier–Stokes equations in the actual channel geometry, are the most accurate and, at the same time, the most computationally expensive, as well as being difficult to solve [4–6]. The one-dimensional (1D) mathematical models formulated under some simplifications in the process description are practically feasible and therefore most often used. In the 1D models both a gas phase species composition and temperature are taken as constant throughout the reactor cross-section, while the temperature and concentration gradients between gas and solid phases are located in a thin film near the surface. At the numerical simulations of the reactive monolith by the 1D models with unsteady-state equations for heat and mass transport, the catalyst surface dynamics is often neglected [7,8]. Veser and Frauhammer [9] used an unsteady-state mathematical model accounting for dynamics of the processes on the catalyst surface, but one simplification was still made: the mass transfer limitation in the boundary layer near the surface was neglected.

If gas phase homogeneous chemical-reactions are included into the mathematical model the axial diffusive transport is important to the flame stabilization mechanism [10]. Furthermore, if molecular weights of species are strongly different, the thermodiffusion transport phenomenon should be taken into account also. Heat transport phenomena by the thermal conductivity of the catalyst matrix [11] and of radiation [12] play a significant role in the high-temperature process as well.

In this paper we studied partial oxidation of methane in a monolith reactor by means of a dynamic 1D reactor model with accounting for detailed molecular, unsteady-state kinetic model for surface reactions. Heat and mass transfer limitations in the boundary layer near the surface, axial diffusion, thermodiffusion, thermal conduction of the solid phase and heat losses due to radiation from the monolith edges are taken into account. The numerical study of the reaction ignition was compared with transient experimental data of start-up to show sufficient relia-

bility of the mathematical model developed. The effect of such parameters as equivalent diameter of the triangular channel, linear velocity and effective thermal conductivity of the monolith on dynamics of the partial oxidation of methane in a shot contact time monolith reactor is also studied.

2. Mathematical model

A 1D reactor model is developed on the base of differential equations of mass and energy changes. The reactor model contains one-dimensional detailed species mass and energy balances both for gas and solid phases, equations for adsorbed species and intermediates. The model implements molecular, non-steady-state kinetics. Accumulation terms were considered in all equations. The following assumptions are considered in the model:

- non-steady-state heat and mass transfer;
- heterogeneously of the system;
- both axial and thermo diffusions in the gas phase;
- thermal conduction of solid phase by means of effective axial thermal conductivity;
- heat loss due to radiation at the reactor inlet and outlet;
- adiabatic monolith reactor (sidewalls of the monolith reactor are isolated).

Model equations, boundary and initial conditions are listed below:

The mass balance equations:

gas phase

$$\varepsilon\frac{\rho_g\partial\omega_i}{\partial t} = -\varepsilon\frac{\rho_g\upsilon\partial\omega_i}{\partial z} - \varepsilon\frac{\partial J_i}{\partial z} - S_{sp}\beta_i(z)\rho_g(\omega_i-\hat{\omega}_i) + \varepsilon\sum_{j=1}^{Nr_g}\nu_{ij}r_j + S_{sp}\omega_i\rho_g\sum_{i=1}^{N_g}\beta_i(z)(\omega_i-\hat{\omega}_i),$$

$$J_i = -\rho_g\frac{M_i}{M_{mix}}D_{im}\frac{\partial x_i}{\partial z} - D_i^T\frac{1}{T}\frac{\partial T}{\partial z}, \quad i=1,N_g \tag{1}$$

solid phase

$$\hat{\varepsilon}\hat{\rho}_g\frac{\partial\hat{\omega}_i}{\partial t} = S_{sp}\beta_i(z)\rho_g(\omega_i-\hat{\omega}_i) + S_s f_{pt}M_i\sum_{j=1}^{Nr_s}\mu_{ij}\hat{r}_j - S_{sp}\hat{\omega}_i\rho_g\sum_{i=1}^{N_g}\beta_i(z)(\omega_i-\hat{\omega}_i) - \hat{\omega}_i S_c f_{pt}\sum_{i=1}^{N_g}M_i\sum_{j=1}^{Nr_s}\mu_{ij}\hat{r}_j, \quad i=1,N_g \tag{2}$$

The energy balance equations:

gas phase

$$\varepsilon\rho_g c_{p_g}\frac{\partial T_g}{\partial t} + \varepsilon\upsilon\rho_g c_{p_g}\frac{\partial T_g}{\partial z} = S_{sp}\alpha(z)(T_s-T_g) - \varepsilon\sum_{j=1}^{Nr_g}\Delta H_j r_j - \varepsilon\sum_{j=1}^{N_g}c_{p_i}J_i\frac{\partial T_g}{\partial z} \tag{3}$$

solid phase

$$(1-\varepsilon)\rho_s c_{p_s}\frac{\partial T_s}{\partial t} = (1-\varepsilon)\frac{\partial}{\partial z}\lambda_{eff}\frac{\partial T_s}{\partial z} - S_{sp}\alpha(z)(T_s-T_g) - S_c f_{pt}\sum_{j=1}^{Nr_s}\Delta H_j\hat{r}_j \tag{4}$$

Species mass balance equations:

$$\frac{\partial\theta_k}{\partial t} = \sum_{j=1}^{Nr_s}\nu_{kj}\hat{r}_j, \quad k=1,N_s \tag{5}$$

Boundary conditions:

$$z=0: \quad T_g=T_{in}; \quad \omega_i=\omega_{i_{in}}; \quad \lambda_{eff}\frac{\partial T_s}{\partial z} = \sigma\varepsilon'(T_s^4-T_w^4);$$
$$z=L: \quad \frac{\partial\omega_i}{\partial z}=0; \quad -\lambda_{eff}\frac{\partial T_s}{\partial z} = \sigma\varepsilon'(T_s^4-T_w^4). \tag{6}$$

Initial conditions:

$$t=0: \quad \omega_i=\omega_i^0; \quad \hat{\omega}_i=\hat{\omega}_i^0; \quad T_s = T_s^0; \quad T_g=T_g^0; \quad \theta_i=\theta_i^0. \tag{7}$$

The changes in a local concentration of the ith component due to mass transport of all components in the system are described by the last term on the right-hand side of Eq. (1) and next to last on the right-hand side of Eq. (2). The last term on the right-hand side of Eq. (2) describes a local concentration changes in the ith component due to participation of all components in surface reactions.

The following dependences are also used:

for mass density in the gas phase

$$\rho_g = \frac{P}{RT_g}M_{mix},$$

for the mixture-averaged diffusion coefficients D_{im} between species i and remaining mixture

$$\frac{1}{D_{im}} = \frac{1}{1-x_i}\sum_{i\neq k}\frac{x_i}{D_{ik}},$$

where D_{ik} is described as (Reid and Sherwood [13])

$$D_{ik} = \frac{0.00100T^{1.75}[((1/M_i)+(1/M_k))]^{1/2}}{P\left[\left(\sum\upsilon'\right)_i^{1/3}+\left(\sum\upsilon'\right)_k^{1/3}\right]^2}.$$

The thermal diffusion coefficient of *i*th component is described by the dependence [14]

$$D_i^{\mathrm{T}} = D_{\mathrm{im}}\omega_i\rho_g\left(\frac{M_i}{M_{\mathrm{mix}}} - 1\right)(2-m)$$

The transport properties via local heat and mass-transfer coefficients $\alpha(\beta)$ were accounted for by the specific heat and mass transfer correlations for Nusselt and Sherwood numbers $Nu(Sh)$ in a triangular channel (Groppi and Tronconi [15]):

$$Nu(Sh) = 2.495 + 6.507(z^*10^3)^{-0.434}\exp(-44.02z^*)$$

The coefficients of diffusions, thermal conductivity and viscosity that depend on composition and temperature were calculated in every axial position along the channel. The heat capacity of the gas flow was calculated against a current composition as:

$$c_p = \sum_i c_{p_i}x_i$$

The heat capacities c_{p_i} were taken at the average temperature [16].

The present study emphasizes the effect of the surface reactions on the process dynamics, so the gas phase reactions are neglected.

3. Unsteady-state kinetic model of surface reactions

The implications of the reliable detail kinetic model for reactor simulation and scale-up are significant. Parameters of elementary steps are often borrowed from surface science experiments whenever available, and the missing (a few) parameters are fitted to a single set of experiments [17]. Similar approach was applied in the development of the kinetic model for the Pt/CeO_2-ZrO_2-La_2O_3/α-Al_2O_3 honeycomb monolith. At first, the literature data [18–20] of partial oxidation of methane over Pt catalyst were used. Detailed heterogeneous chemistry mechanism proposed by Aghalayam et al. [19] includes all possible species transformations on the Pt catalyst. The reaction mechanism contains 31 elementary steps describing methane oxidation on platinum, 14 gaseous compounds and 11 intermediates. The authors have carefully listed all necessary parameters for the quantitative description of kinetics and heat effects in every elementary step of the surface mechanism. However, some dis-

Table 1
Surface reaction mechanism for oxidation of methane over Pt/Ce-Zr-La/α-Al_2O_3

No.	Reaction	k_f preexponential (s^{-1}) or sticking coefficient	E_f (kcal/mol)	k_b preexponential (s^{-1})	E_b (kcal/mol)	$\Delta_r H$ (kcal/mol)
1	$OH^* + * \leftrightarrow H^* + O^*$	5.60×10^{11}	18.3	1.70×10^{10}	13.4	4.9
2	$H_2O^* + * \leftrightarrow H^* + OH^*$	1.20×10^{10}	39.1	3.50×10^{11}	0.0	39.4
3	$H_2O^* + O^* \leftrightarrow 2OH^*$	1.00×10^{11}	34.1	1.00×10^{11}	0.0	34.1
4	$H_2 + 2^* \leftrightarrow 2H^*$	0.09	0.0	3.33×10^{12}	20.0	−16.0
5	$O_2 + 2^* \leftrightarrow 2O^*$	0.03	0.0	1.00×10^{11}	19.0	−15.0
6	$H_2O + * \leftrightarrow H_2O^*$	1.00	0.0	5.33×10^{12}	10.0	−10.0
7	$OH + * \leftrightarrow OH^*$	1.00	0.0	1.00×10^{13}	30.0	−30.0
8	$H + * \leftrightarrow H^*$	1.00	0.0	1.00×10^{13}	60.2	−60.2
9	$O + * \leftrightarrow O^*$	1.00	0.0	1.00×10^{13}	67.0	−67.0
10	$CH_4 + 2^* \leftrightarrow CH_3* + H^*$	0.68	12.0	3.97×10^{10}	5.5	6.5
11	$CH_3^* + * \leftrightarrow CH_2^* + H^*$	1.32×10^{13}	25.8	4.04×10^{10}	6.1	19.7
12	$CH_2^* + * \leftrightarrow CH^* + H^*$	1.00×10^{11}	25.0	1.00×10^{11}	12.2	12.8
13	$CH^* + * \leftrightarrow C^* + H^*$	1.00×10^{11}	5.4	1.00×10^{11}	37.6	−31.4
14	$CH_3^* + O^* \leftrightarrow CH_2^* + OH^*$	1.00×10^{11}	17.7	1.00×10^{11}	3.1	14.6
15	$CH^* + OH^* \leftrightarrow CH_2^* + O^*$	1.00×10^{11}	13.2	1.00×10^{11}	20.5	−7.3
16	$C^* + OH^* \leftrightarrow CH^* + O^*$	1.00×10^{11}	38.2	1.00×10^{11}	1.5	36.7
17	$CH_2^* + H_2O^* \leftrightarrow CH_3^* + OH^*$	1.00×10^{11}	19.5	1.00×10^{11}	0.0	19.5
18	$CH^* + H_2O^* \leftrightarrow CH_2^* + OH^*$	1.00×10^{11}	26.7	1.00×10^{11}	0.0	26.7
19	$C^* + H_2O \leftrightarrow CH^* + OH^*$	1.00×10^{11}	70.9	1.00×10^{11}	0.0	70.9
20	$CO^* + * \leftrightarrow C^* + O^*$	1.00×10^{11}	74.2	1.00×10^{11}	0.0	75.
21	$CO_2^* + * \leftrightarrow CO^* + O^*$	1.00×10^{11}	43.1	1.00×10^{11}	0.0	43.1
22	$CO + ^* \leftrightarrow CO^*$	0.71	0.0	1.00×10^{13}	34.0	−34.0
23	$CO_2 + * \leftrightarrow CO_2^*$	0.7	0.0	1.00×10^{12}	17.0	−17.0
24	$CO_2^* + H^* \leftrightarrow CO^* + OH^*$	1.00×10^{11}	38.2	1.00×10^{11}	0.0	38.2
25	$CO^* + H^* \leftrightarrow CH^* + O^*$	1.00×10^{11}	106.0	1.00×10^{11}	0.0	106.0
26	$CO^* + H^* \leftrightarrow C^* + OH^*$	1.00×10^{11}	69.2	1.00×10^{11}	0.0	69.2
27	$CH_3 + * \leftrightarrow CH_3^*$	1.00	0.0	1.00×10^{13}	38.0	−38.0
28	$CH_2 + * \leftrightarrow CH_2^*$	1.00	0.0	1.00×10^{13}	68.0	−68.0
29	$CH + * \leftrightarrow CH^*$	1.00	0.0	1.00×10^{13}	97.0	−97.0
30	$C + ^* \leftrightarrow C^*$	1.00	0.0	1.00×10^{13}	150.0	−149.0
31	$2CO^* \leftrightarrow C^* + CO_2^*$	2.40×10^{12}	31.0	4.17×10^{9}	0.0	31.9
32	$O^* + Z \leftrightarrow *+ZO$	0.2×10^{3}	1.4	0.2×10^{3}	1.4	0.0

The site densities were assumed: for the Pt, 1.65×10^{-5} mol/m^2 and for ZO, 1.65×10^{-2}.

crepancy was found to be in both the enthalpies and equilibrium constants for the main reaction routes. For example, for a reaction rout $CH_4 + 0.5O_2 \rightarrow CO + 2H_2$ consisted of the steps 4, 5, 10, 11, 12, 13, 20, 22, the value for the heat evolved was $\Delta_r H = +6.6$ kcal/mol instead of -8.51 kcal/mol calculated on base of the thermodynamics laws. After some corrections, the mechanism proposed by Aghalayam et al. [19] was taken as a basis for the unsteady-state kinetic model to be implemented in the dynamic reactor model developed. The implemented detailed mechanism containing 32-elementary-step of methane oxidation, 14 gaseous compounds and 13 intermediates on the catalyst surface with corresponding kinetic parameters is given in Table 1.

The Pt/Ce-Zr-(La)/α-Al_2O_3 honeycomb monolith is a complex catalytic system where washcoat (fluorite-like nanocrystallites of solid solution CeZr/CeZrLa) closely interacts with active component Pt. Study of detailed kinetic and mechanism of the partial oxidation reaction using the step response technique has made it clear that active oxygen of the bulk quickly re-oxidizes the reduced platinum [21]. The simplified reaction scheme illustrates the reaction mechanism over Pt/CeO_2-ZrO_2 catalyst:

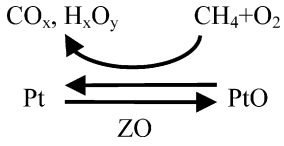

The unsteady-state kinetic models of the partial oxidation of methane over both Pt/CeO_2-ZrO_2/α-Al_2O_3 and Pt/CeO_2-ZrO_2-La_2O_3/α-Al_2O_3 monoliths account for the interaction of washcoat (Z, ZO) with active catalyst sites (Pt, PtO) (reaction 32 in Table 1). The difference between both catalysts consists in the amount of active sites and numerical values for the kinetic parameters of the reaction elementary steps.

4. Development of the numerical algorithm

The model balance equations form a set of differential equations in partial derivatives. An efficient robust algorithm was developed for solving the system.

A method of lines was used to treat the system numerically. Discrete approximation of differential operators on the spatial variable, functions of reactions, heat and mass exchange terms and boundary conditions was based on the mass and heat conserving integro-interpolation method [22]. Integral form of the equations was applied at each increment $[z_{l-1/2}, z_{l+1/2}]$ of the axial direction. A reaction term in the mass balance equations was represented as a sum of two terms to extract a linear part with respect to the *i*th component. This allows the assigned linear part to be transferred to diagonal of the system, thus increasing a monotony of the system and securing non-negativity of the concentrations [23]. As a result, a large system of the non-linear ordinary differential equations was obtained. The methods of Gauss–Seidel iterations and a second-order Rozenbroke algorithm with an automatic choice of the integration interval were used to solve the set of equations [24]. The Fortran computed code was developed to implement the algorithm described.

5. Start-up experiments procedure

The start-up (light-off) experiments for the partial oxidation of methane over the Pt/CeZrLa deposited onto the alumina based monolith were carried out in a flow reactor. The catalyst was prepared according to procedures described in References [3,21,25]. The reactor consisted of a 25 cm long quartz tube with an internal diameter of 60 mm and equipped with several thermocouple wells. Honeycomb monolith with following parameters: a hexagonal side of 28 mm, monolith length of 50 mm, wall thickness of 0.25 mm, equivalent channel diameter of 1.9 mm, surface area of 3–10 m^2/g, was employed in the experiments. Unloaded monoliths were placed in front of and behind the catalyst to reduce radiation heat loss. A ceramic cloth wound around the catalyst, 1 mm thick, prevented gas bypass. Chromel–alumel thermocouples were used to monitor gas temperature at various positions along the catalyst axis. The reactor was operated at atmospheric pressure. In 56.7% N_2 dilution, CH_4 and O_2 with a molar ratio of 1.76 were fed at 673 K into the preheated monoliths with flow rate of 3.5 to 5.5 × 10^3 l(n)/h. The product composition was determined by gas chromatography (GC) and quadrupole mass spectroscopy (QMS). The latter was applied for transient measurements such as the ignition experiment of this study. A furnace was used to ignite the reaction by heating up the monolith using a temperature ramp of 5 K/min. As soon as ignition occurred, the furnace was turned off.

6. Results and discussion

6.1. Comparison of modeling results and experimental data

Due to the high-temperature operating conditions and the typically very fast chemistry of oxidation reactions, a *direct* experimental investigation of all steps of the reaction mechanism is difficult if possible at all under realistic conditions. Therefore, simulation studies could be also used to elucidate both the underlying mechanism and kinetic parameters. To achieve this, the reactor model coupled with the detailed elementary step unsteady-state kinetic model was applied to test the simulation results against available transient experimental data of the reaction ignition during start-up. Due to their high sensitivity to the specific reaction path taken during the transient excursion of the reaction system, good correlations in such comparison approve a reliability of the mathematical model applied [9,26–30].

The experimental data with the full-scale hexagonal corundum extruded monoliths with triangular shape channels washcoated by the 0.4% platinum on ceria-zirconia-lanthanum fluorite-like solid solution were taken for the comparison with the numerical results.

The numerically predicted gas phase axial temperature profiles in the Pt/CeO_2-ZrO_2-La_2O_3 monolith as the functions of time (curves) in comparison with the measurements (symbols) are revealed in Fig. 1. Generally, the simulation is in good agree-

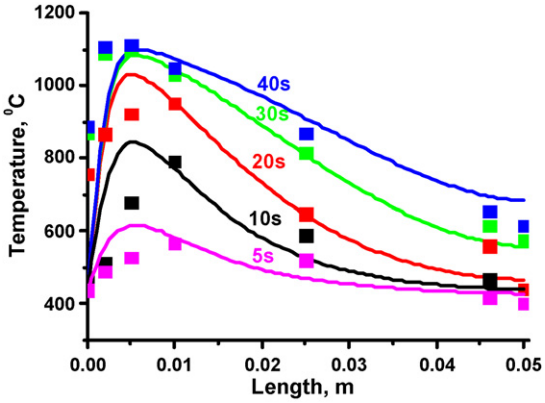

Fig. 1. Gas temperature evolution during start-up. Feed mixture: 0.24 mole fraction of CH_4 in air, $T = 420\,^{\circ}C$, $P = 1$ atm, $u = 0.5$ m(n)/s. Lines, modeling predictions; symbols, experimental data.

ment with the experimental results, yet for the first 20 s the predicted temperature in the front part of the monolith increases slightly faster than the experimentally measured temperature. During this time the hottest part was found to be at the length of 0.01 m in the experiment and at 0.005 m in the simulations. The error bar of the measurements certainly existed, but the slower temperature rise in the experiments in comparison with the 2D modeling data was also noted by Schwiedernoch et al. [29]. These authors assumed that that was due to the heat capacity of the thin quartz tube, in which the thermocouple was placed. There were no the quartz tubes in the experiments in our case. Other reasons of both chemical and transport nature could be advanced. In addition, the start-up behavior is also dependent on a prehistory of the catalyst. To clarify the matter discussed a special study will be undertaken.

In Fig. 2, the numerically predicted concentrations of components in the product gas (Fig. 2a) are compared with the experimentally derived data (Fig. 2b). Again, a fair qualitative agreement between the measured and simulated species profiles is observed. There are almost no both CO and H_2 at the ignition point, the total oxidation to CO_2 occurs at first. The concentration of CO_2 goes through a maximum in both the numerical and real experiments. On the contrary to the data derived from the experiment with the rhodium coated monolith [29], where CO formation starts before hydrogen formation, hydrogen is detected first during at the ignition of Pt/Ce-Zr-La/α-Al_2O_3 monolith. And again, the simulated gas phase composition reaches steady-state faster than it was in the transient experiment. This fact was also observed by Schwiedernoch et al. [29]. As to quantitative agreement between the data discussed, the model slightly overestimates CO_2 concentration due to the high rate of the water gas shift reaction route. It might be due to the fact that transient kinetic experiments were carried out with the massive Pt/Ce-Zr-La catalyst [20], while the washcoated monolith Pt/Ce-Zr-La/α-Al_2O_3 was used in the transient experiment. Despite of the deviations mentioned, the results of the numerical experiments are in sufficient agreement with the experimental data, thus indicating that the model developed is reliable enough to be used for the numerical study of the partial oxidation of methane over Pt/Ce-Zr-La/α-Al_2O_3 monolith.

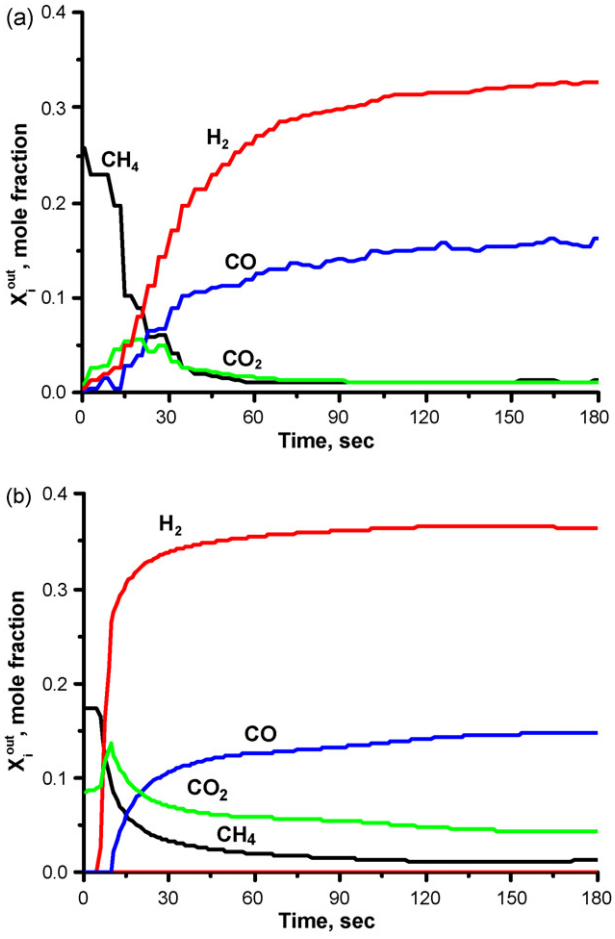

Fig. 2. Time dependencies of main components in the product gas. Feed mixture: 0.267 mole fraction of CH_4 in air, $T = 400\,^{\circ}C$, $P = 1$ atm, $u = 0.34$ m(n)/s. (a) Experimental data and (b) modeling results.

6.2. The numerically predicted temperature and concentrations profiles

The numerically predicted distribution of the temperature (a) and gas phase molar fractions (b–d) and coverage of the free surface sites (f) in the monolith as a function of time is shown in Fig. 3. During first 5 s total oxidation of CH_4 to CO_2 and H_2O occurs (Fig. 3a and b), due to which the temperature in the front part of the monolith is sharply increased. There is no CO (Fig. 3c) and H_2 (Fig. 3d) produced in the first few second after ignition. At 5 s the temperature (Fig. 3e) is high enough for hydrogen formation, and CO appears in 2 s later. Complex dynamic behavior of the surface species is revealed. Fig. 3f shows that at the very short times dramatic changes in the surface coverage occur, the vacancies coverage reaches steady-state rather slowly due to the multi-step heterogeneous reaction mechanism. The adsorption–desorption equilibrium of the species shifts with increasing the temperature leading to changing the rate-limiting steps and prevailing reaction routes in the surface reaction kinetics. Calculated molar gas phase concentrations at steady-state of methane oxidation in the monolith reactor are showed in Fig. 4. It can be seen that the conversion of oxygen reaches completion after 10% of length behind the monolith

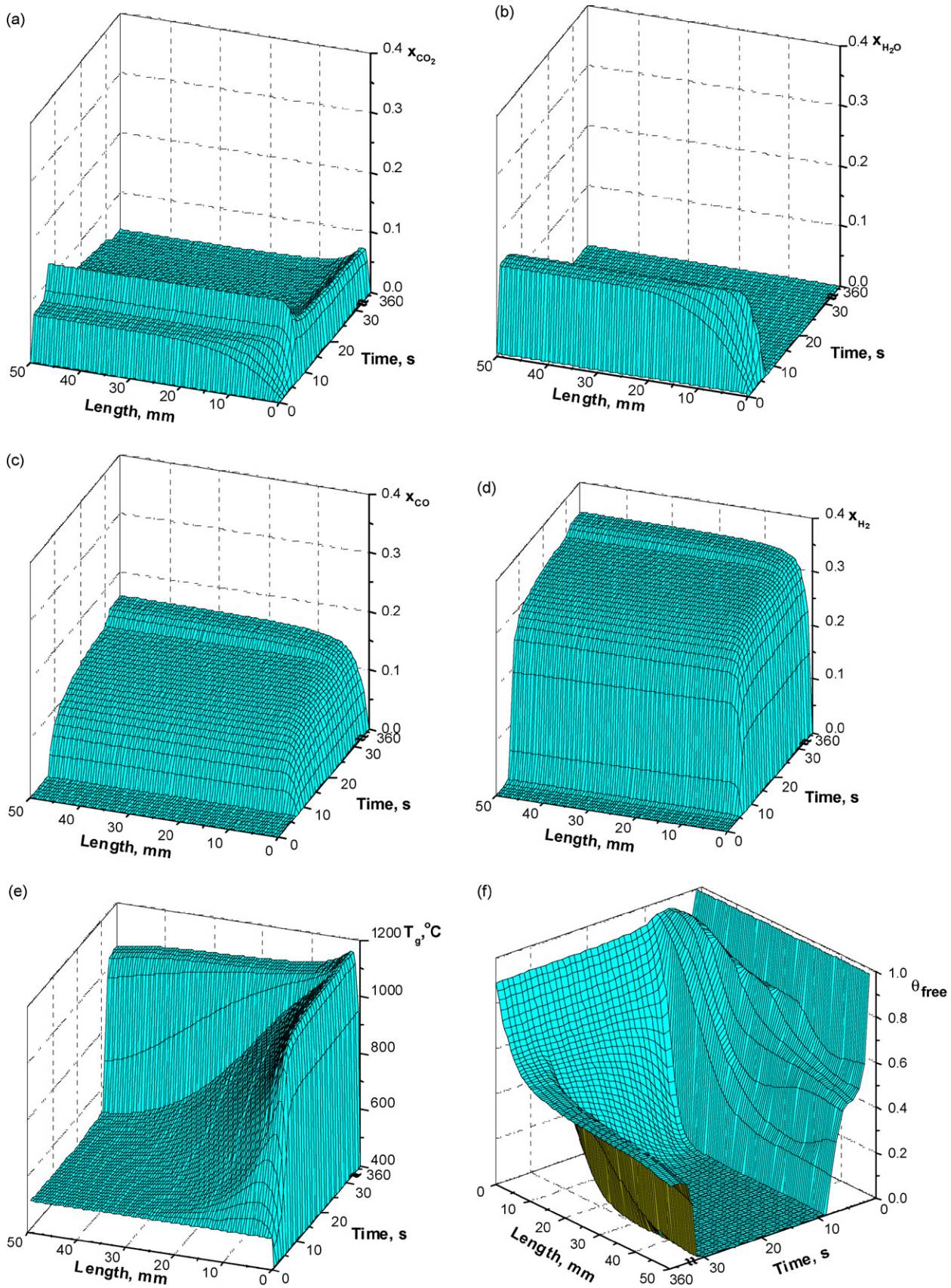

Fig. 3. Catalytic ignition in the honeycomb monolith with triangular channel cross-section. Feed mixture: 0.25 mole fraction of CH_4 in air, $T = 400\,^{\circ}C$, $P = 1$ atm, $u = 0.3$ m(n)/s, $d_{eq} = 0.67$ mm, $\varepsilon = 0.59$. (a and b) Mass fraction of the total oxidation products (CO_2 and H_2O); (c and d) mass fraction of the partial oxidation products (CO and H_2); (e) temperature; (f) free surface sites.

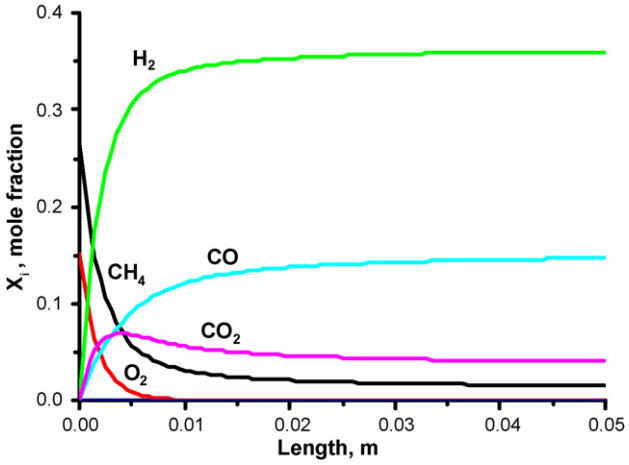

Fig. 4. Axial steady-state profiles of molar fractions in gas phase. Feed mixture: 0.267 mole fraction of CH_4 in air, $T = 400\,^{\circ}C$, $P = 1$ atm, $u = 0.34$ m(n)/s.

entrance. The length of the oxidation zone depends on both a superficial velocity and stoichiometry of the reactants. Methane concentration drops with the same rate as long as oxygen is present, and keeps decreasing slowly downstream. Some CO_2 is formed in the oxidation zone, the concentration plot goes through the maximum and gradually diminishes toward the end of the catalyst bed. All most important changes in the concentrations of gas phase species, including those for the desired products—H_2 and CO, occur in the oxidation zone. The numerical predictions are in a good qualitative consistency with the first experimentally measured species profiles for methane partial oxidation on Rh-coated foams [31]. However, the published data indicate clearly that the gas phase reactions with consumption of oxygen and formation of water occur before the catalyst edge. Obviously, hydrogen diffusion following by reaction with incoming oxygen does exist. This motivates a further work on the reactor model.

6.3. The influence of the process parameters on the start-up dynamics

The influence of such parameters as linear velocity, equivalent channel diameter and effective thermal conductivity of the monolith on the ignition dynamics in the methane partial oxidation process has been also studied. Duration of the start-up period, a delay in syngas production after a moment of feeding the reagents into the preheated monolith, is very important to know in many applications. According to the numerical predictions with the model adopted in this work, for a given operational parameters the time delay in syngas production during the light-off decreases from 18 to 6 s with increasing equivalent diameter (d_{eq},) of the triangular channel from 0.38 to 0.67 mm, as shown in Fig. 5. In case of the higher channel diameter, the initial rapid increase in the temperature in the entrance zone is predicted due to the large amount of heat release, which allows minimizing the time delay. However, at steady-state the worse interphase transport properties in the monolith result in the lower temperature along the monolith axis, methane conversion, and CO selectivity, while slightly higher H_2 selectivity is calculated.

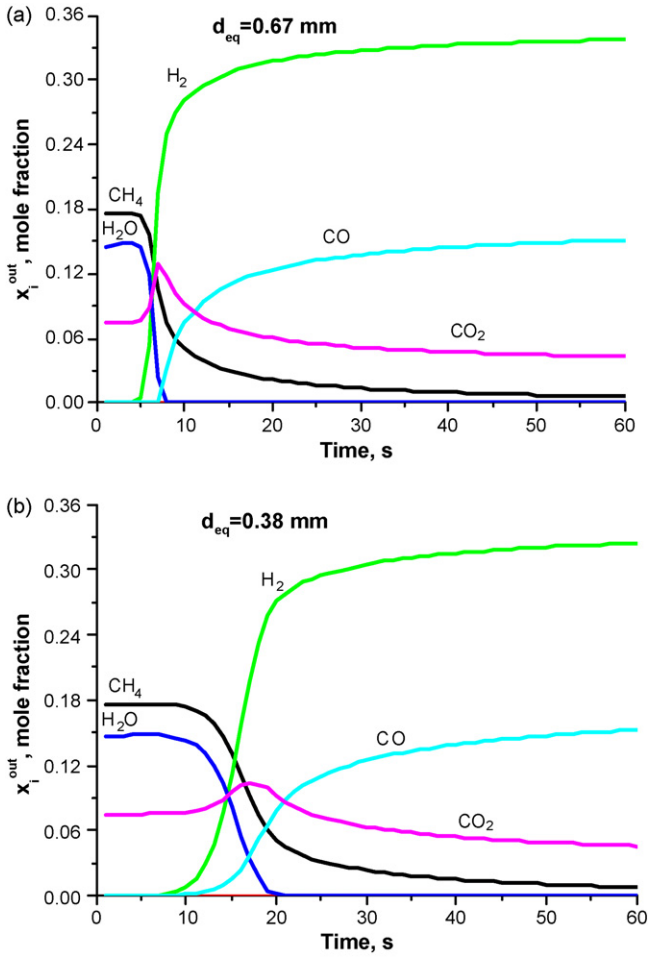

Fig. 5. Effect of equivalent diameter of the triangular channel on the time delay in syngas production during ignition. Feed mixture: 0.25 mole fraction of CH_4 in air, $T = 400\,^{\circ}C$, $P = 1$ atm, $u = 0.3$ m(n)/s, $\varepsilon = 0.59$. (a) $d_{eq} = 0.67$ mm and (b) $d_{eq} = 0.38$ mm.

The dynamics of the temperature in the monolith are driven by both the heat release in the surface reactions and heat removal due to the gas–solid convective heat transfer [32]. Increasing linear velocity favors decreasing the start-up period due to the large amount of heat evolved in the reaction zone. As the rate of mass transfer controls O_2 consumption in the hot spot, a more sharp temperature profile is formed along the reactor axis in the steady-state mode, while the outlet temperature is found to be lower for the given conditions with the corresponding negative effect on both methane conversion and CO selectivity, while selectivity to hydrogen is improved.

The results of the numerical experiments with the axial channel conductivity varied are in line with the finding published elsewhere [33,34]: increasing the conductivity smoothens the temperature peak in the channel. However, this may results in the higher value for the time delay in syngas production during start-up.

7. Conclusions

A monolith short-contact time syngas reactor is simulated using a dynamic mathematical model with detailed molecu-

lar, unsteady-state kinetic model for surface reactions of the methane partial oxidation over Pt/Ce-Zr-La catalyst. The 1-D model developed enables the underlying physics of the process to be captured and not only to explain but also to predict a transient behavior of the monolith reactor. Both algorithm and numerical codes were developed as well. The model was applied to test the simulation results against available transient experimental data of the reaction ignition in a full-scale hexagonal corundum extruded monoliths with triangular shape channels. In spite of some differences observed, rather good correlations were obtained that encouraged both the present and future numerical study of the process dynamics by using the reactor model developed. Also studied is the influence on the ignition dynamics such parameters as linear velocity, equivalent channel diameter and effective thermal conductivity of the monolith. It was found that increasing linear velocity and equivalent channel diameter as well as decreasing axial conductivity of solid phase favors decreasing a time delay in syngas production in the Pt/Ce-Zr-La/α-Al_2O_3 honeycomb monolith with a triangular shape channels.

Further work will be carried out on the refinement of the mathematical model of the methane partial oxidation process in a monolith reactor, to account for the gas phase reactions, particularly, in the frontal part of the catalyst.

Acknowledgements

This work is in part supported by ISTC 2529 and RFBR 060381037 Projects. The authors thank L.L. Gogin, T.A. Nikoro, Z.Yu. Vostrikov for presented experimental data and E.M. Sadovskaya for fruitful discussion.

References

[1] R.P. O'Connor, E.J. Klein, L.D. Schmidt, High yields of synthesis gas by millisecond partial oxidation of higher hydrocarbons, Catal. Lett. 70 (2000) 99–107.
[2] L.D. Schmidt, Modeling millisecond reactions, in: Studies in Surf. Sci. and Catalysis vol. 136. Natural Gas Conversion VI: Proc. Of the 6th Natural Gas Conversion Symposium, Alaska, June 17–22, 2001.
[3] L. Bobrova, I. Zolotarskii, V. Sadykov, S. Pavlova, O. Snegurenko, S. Tikhov, V. Korotkich, T. Kuznetsova, V. Sobyanin, V. Parmon, Syngas formation by selective catalytic oxidation of liquid hydrocarbons in a short contact time adiabatic reactor, Chem. Eng. J. 107 (2005) 171–179.
[4] O. Deutschmann, L.D. Schmidt, Modeling the partial oxidation of methane in a short contact time reactor, AIChE J. 44 (11) (1998) 2465–2477.
[5] M.J. Stutz, N. Hotz, D. Poulikakos, Optimization of methane reforming in a microreactor—effect of catalyst loading and geometry, Chem. Eng. Sci. 61 (2006) 4027–4040.
[6] A. Schneider, J. Montzaras, P. Jansohn, Experimental and numerical investigation of the catalytic partial oxidation of CH_4/O_2 mixture diluted with H_2O and CO_2 in a short contact time reactor, Chem. Eng. Sci. 61 (2006) 4634–4649.
[7] D.A. Hichman, L.D. Schmidt, Steps in CH_4 oxidation on Pt and Rh surfaces: high-temperature reactor simulations, AIChE J. 39 (7) (1993) 1164–1177.
[8] P. Aghalayam, Y.K. Park, D.G. Vlachos, Partial oxidation of light alkanes in short contact time microreactors, Catalysis (15) (2000) 98–137.
[9] G. Veser, J. Frauhammer, Modelling steady state and ignition during catalytic methane oxidation in a monolith reactor, Chem. Eng. Sci. 55 (2000) 2271–2286.
[10] L.L. Raja, R.J. Kee, O. Deutschmann, J. Warnatz, L.D. Schmidt, A critical evaluation of Navier-Stokes, boundary-layer, and plug-flow model of the flow and chemistry in a catalytic-combustion monolith, Catal. Today 59 (2000) 47–60.
[11] G. Groppi, E. Tronconi, Honeycomb support with high thermal conductivity for gas/solid chemical processes, Catal. Today 105 (2005) 297–304.
[12] A.D. Benedetto, S. Cimino, R. Pirone, G. Russo, Temperature excursions during the transient behaviour of high temperature catalytic combustion monoliths, Catal. Today 83 (2003) 171–182.
[13] R.C. Reid, T.K. Sherwood, The Properties of Gases and Liquids, McGraw-Hill Book Company, 1966.
[14] D.A. Frank-Kamenetsky, Diffusion and Heat Transfer in Chemical Kinetics, Nauka, Moscow, 1987 (in Russian).
[15] G. Groppi, E. Tronconi, Theoretical analysis of mass and heat transfer in monolith catalyst with triangular channels, Chem. Eng. Sci. 52 (20) (1997) 3521–3526.
[16] John H. Perry. Chemical Engineers's Handbook. McGraw-Hill Book Company, New York.
[17] S. Raimondeau, D.G. Vlachos, Recent developments on multiscale, hierarchical modeling of chemical reactors, Chem. Eng. J. 90 (2002) 3–23.
[18] D.A. Hickman, L.D. Schmidt, Steps in CH4 oxidation on Pt and Rh surfaces: High-temperature reactor simulations, AIChE J. 39 (1993) 1164–1177.
[19] P. Aghalayam, Y.K. Park, N. Fernandes, V. Papavassiliou, A.B. Mhadeshwar, D.G. Vlachos, A C1 mechanism for methane oxidation on platinum, J. Catal. 213 (2003) 23–38.
[20] K.A. Willams, C.A. Leclere, L.D. Schmidt, Rapid lightoff of syngas production from methane: a transient product analysis, AIChE J. 51 (1) (2005) 247–260.
[21] C. Mirodatos, Y. Schuurman, A.C. van Veen, V.A. Sadykov, L.G. Pinaeva, E.M. Sadovskaya, Investigation of unsteady-state redox mechanisms over ceria based catalysts for partial oxidation of methane, in: Natural Gas Conversion VIII: Proceedings of the 8th Natural Gas Conversion Symposium, Natal, Brazil, Stud. Surf. Sci. Catal. vol. 167 (May 27–31, 2007).
[22] A.A. Samarskii, A.P. Mikhailov, Mathematical modeling: Ideas, Methods, Examples, Moscow, 2001 (in Russian).
[23] L.A. Rapatski, L.V. Yausheva, Mathematical modeling of catalytic processes in porous medium, Preprint No 1019. Novosibirsk, 1994 (in Russian).
[24] E.A. Novikov, Numerical methods for solution of differential equations in chemical kinetics, in: Mathematical Methods in Chemical Kinetics, Nauka, Novosibirsk, 1990, pp. 53–68 (in Russian).
[25] V.A. Sadykov, S.N. Pavlova, R.V. Bunina, G.M. Alikina, S.F. Tikhov, T.G. Kuznetsova, Yu.V. Frolova, A.I. Lukashevich, O.I. Snegurenko, N.N. Sazonova, E.V. Kazantseva, Yu.N. Dyatlova, V.V. Usol'tsev, I.A. Zolotarskii, L.N. Bobrova, V.A. Kuz'min, L.L. Gogin, Z.Yu. Vostrikov, Yu.V. Potapova, V.S. Muzykantov, E.A. Paukshtis, E.B. Burgina, V.A. Rogov, V.A. Sobyanin, V.N. Parmon, Selective oxidation of hydrocarbons into synthesis gas at short contact times: design of monolith catalysts and main process parameters, Kinet. Catal. 46 (2) (2005) 227–250.
[26] G. Veser, L.D. Schmidt, Ignition and extinction in the catalytic oxidation of hydrocarbons over platinum, AIChE J. 42 (1996) 1077–1987.
[27] P.-A. Bui, D.G. Vlachos, P.R. Westmoreland, Catalytic ignition of methane/oxygen mixtures over platinum surfaces: comparison of detailed simulations and experiments, Stud. Surf. Sci. Catal. 385 (2–3) (1997) L1029–L1034.
[28] O. Deutschmann, R. Schmidt, F. Behrendt, J. Warnatz, Numerical Modeling of Catalytic Ignition, in: Twenty Sixth Symposium (International) on Combustion, The Combustion Institute, Pittsburgh, 1996, pp. 1747–1754.
[29] G.R. Schwiedernoch, S. Tischer, C. Correa, O. Deutschmann, Experimental and numerical study of the transient behavior of a catalytic partial oxidation monolith, Chem. Eng. Sci. 58 (3–6) (2003) 633–642.
[30] F. Behrendt, O. Deutschmann, R. Schmidt, J. Warnatz, Ignition and extinction of hydrogen–air and methane air mixtures over platinum and palladium, in: B.K. Warren, S.T. Oyama (Eds.), Heterogeneous Hydro-

carbon Oxidation ACS Symposium Series, vol. 638, American Chemical Society, 1996, pp. 49–57.
[31] R. Horn, K.A. Williams, N.J. Degenstein, L.D. Schmidt, Syngas by catalytic partial oxidation of methane on rhodium: Mechanistic conclusions from spatially resolved measurements and numerical simulations, J. Catal. 242 (2006) 92–102.
[32] M. Maestri, A. Beretta, G. Groppi, E. Tronconi, P. Forzatti, Comparison among structured and packed-bed reactors for the catalytic partial oxidation of CH_4 at short contact times, Catal. Today 105 (2005) 709–717.
[33] G. Groppi, E. Tronconi, Simulation of structures catalytic reactors with enhanced thermal conductivity for selective oxidation reactions, Catal. Today 69 (2001) 63–73.
[34] Th. Boger, A.K. Heibel, Heat transfer in conductive monolith structures, Chem. Eng. Sci. 60 (2005) 1823–1835.